

CrystEngComm

Accepted Manuscript



This is an *Accepted Manuscript*, which has been through the Royal Society of Chemistry peer review process and has been accepted for publication.

Accepted Manuscripts are published online shortly after acceptance, before technical editing, formatting and proof reading. Using this free service, authors can make their results available to the community, in citable form, before we publish the edited article. We will replace this *Accepted Manuscript* with the edited and formatted *Advance Article* as soon as it is available.

You can find more information about *Accepted Manuscripts* in the [Information for Authors](#).

Please note that technical editing may introduce minor changes to the text and/or graphics, which may alter content. The journal's standard [Terms & Conditions](#) and the [Ethical guidelines](#) still apply. In no event shall the Royal Society of Chemistry be held responsible for any errors or omissions in this *Accepted Manuscript* or any consequences arising from the use of any information it contains.

Cite this: DOI: 10.1039/c0xx00000x

www.rsc.org/xxxxxx

ARTICLE TYPE

Growth mechanism and PL properties of β -Sialon nanobelts/nanowires synthesized in process of aluminothermic reduction nitridation of zirconHaitao Liu,^a Fanrong Meng,^{c,d} Qing Li,^{c,d} Zhaohui Huang,^{*a} Shunqin Luo,^b Li Yin,^a Minghao Fang,^{*a} Yan-gai Liu^a and Xiaowen Wu^a

5 Received (in XXX, XXX) Xth XXXXXXXXX 20XX, Accepted Xth XXXXXXXXX 20XX
DOI: 10.1039/b000000x

Large scale β -Sialon nanobelts/nanowires and ZrN-Sialon composite powders were prepared via aluminothermic reduction nitridation at different conditions with flowing N₂. The phase composition, morphology, and microstructure of the as-prepared products were characterized
10 by X-ray diffraction (XRD), field emission scanning electron microscopy (FESEM), transmission electron microscopy (TEM/HRTEM), Fourier-transform infrared spectroscopy (FT-IR) and energy dispersive X-ray spectroscopy (EDS). The experiment results show that the phase compositions and the ratio of nanostructures to powder can be tailored by the experimental conditions. The formation of β -Sialon nanostructures was dominated by a vapor-solid (VS)
15 mechanism. The photoluminescence spectrum of the β -Sialon nanostructures exhibits a special emission peak located in the violet-blue spectral range, making possible potential applications in blue-light emitting diodes and display devices. This process also supplied a feasible way to prepare reinforcing β -Sialon nanostructures *in situ* within the ZrN-Sialon composite powders.

Introduction

20 One-dimensional (1-D) nanostructures materials have attracted extensive attention because of their outstanding properties and potential applications in nano-scaled optoelectronics, sensors, electronics and other functional applications.¹⁻⁵ Sialon is a group of materials consisting of Si, Al, O and N, in which Si-N bonds
25 are partially replaced by Al-O bonds respectively based on the Si₃N₄ structure.⁶ The easy doping property also makes Sialon material demonstrate more extensive applications in optoelectronics.⁷⁻¹⁰ In recent years, various β -Sialon nanostructures have been synthesized such as nanowires,
30 nanobelts and hierarchical nanostructures.^{6,11} Dong *et al.* fabricated two kinds of β -Sialon nanostructures whiskers, rod-like and wool-like whiskers by pressure-less sintering of silicon, aluminum and alumina powders.¹² Huang *et al.* have synthesized
35 nanostructures via a thermal-chemical vapor deposition process using an appropriately selected catalyst.¹¹ However, literatures about 1-D β -Sialon nanostructures are still deficient.

Nitride ceramics are defined as a kind of promising materials as a result of their high melting point, high hardness and strength,
40 excellent chemical and thermal stabilities, good wear resistance, *etc.*¹³⁻¹⁸ The ZrN-based ceramics are a potential candidate for high temperature applications such as refractory material, hard coatings for cutting tools and Josephson junctions in electronics
45 due to its superior properties.¹⁹⁻²² However, intrinsic brittleness is one of the biggest limitations for the application of these inorganic ceramics. Lots of efforts have been devoted to

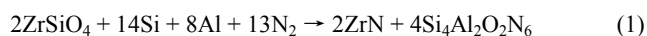
improving their toughness.²²⁻²⁴ *In situ* forming interlocked elongated microstructures or introducing second reinforcing phases (whiskers, fibers or particles) is one of the most important
50 manners.²⁵⁻²⁷ Although significant progresses have been made, further methods of improving the toughness of ceramics is still desired. To the best of our knowledge, no researches synthesized β -Sialon nanostructures with synchronistic preparation of ZrN-Sialon composite powders via aluminothermic reduction
55 nitridation.

On the basis of efficiency and economy, the aluminothermic reduction nitridation is considered to be a potential method for the synthesis of nitride ceramics on account of its inexpensiveness and simplicity. In this paper, 1-D β -Sialon
60 nanostructures were prepared on the graphite felt around the samples in large scale under different conditions. Furthermore, ZrN-Sialon composite powders were also synthesized via an aluminothermic reduction nitridation method with *in situ* formed β -Sialon nanostructures. The microstructure variation of the as-
65 prepared products (the nanostructures and composite powders) was studied with the emphasis on the relationship between microstructure and the heat treatment temperatures. The as-prepared β -Sialon nanostructures grown on the graphite substrate may have potential applications in blue-light emitting diodes and
70 display devices. Moreover, the received composite powders can be useful for preparing nanostructure reinforced ZrN-Sialon composite ceramics.

Experimental

The synthesis of β -Sialon nanostructures and ZrN-Sialon

composite powders was carried out in a high-temperature vacuum furnace via aluminothermic reduction nitridation method. The starting powders were zircon (ZrSiO_4 , purity 98.5%, Yongbang zirconium industry Co. Ltd., Shandong, China), Aluminum powder (purity 99.5%, Sinopharm Chemical Reagent Co. Ltd., Beijing, China), and Silicon powder (purity 99.0%, Sinopharm Chemical Reagent Co. Ltd., Beijing, China). Based on Equation (1), the mass ratio of the precursor materials was revealed in Table 1 as S1. Then 5, 10, 15, 20 and 25 wt% excessive aluminum powder was added to the mixture, noted as S2, S3, S4, S5 and S6.

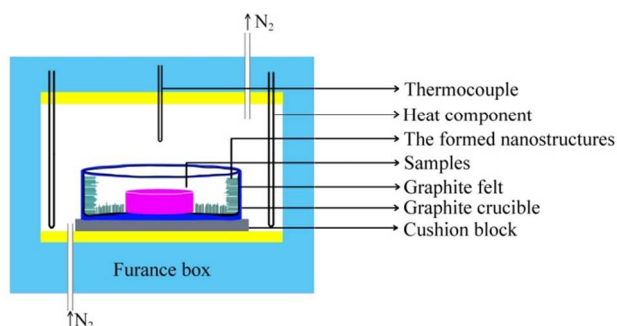


The predetermined amounts of the material powders were mixed in a polytetrafluoro ethylene pot for 12 h and agate balls used as a milling medium. After milled, the as-treated powder mixtures were pressed into cylinder pellets of 20 mm diameter and 8-10 mm height under 20 MPa. The specimens were then placed in a graphite crucible and sintered in a MoSi_2 electrical furnace in a high-purity nitrogen atmosphere at temperatures ranging from 1400 to 1600 °C at an interval of 100 °C. The procedure of sintering was in a programmed manner: first from room temperature to 300 °C in manual-control, then from 300 °C to 1000 °C at 10°C per minute, and then from 1000 °C to the final firing temperature at 5 °C per minute. The sample S1 was held for 4 h at 1400 °C, 1500 °C and 1600 °C. The samples S2, S3, S4, S5 and S6 were sintered at 1600 °C for 4 h. Scheme 1 illustrates the schematic experimental setup of such a process.

Table 1 The mass ratio of the precursor materials.

Sample No.	The mass ratio of the precursor materials		
	ZrSiO_4	Al	Si
S1	3.76	2.22	4.02
S2	3.76	2.33	4.02
S3	3.76	2.44	4.02
S4	3.76	2.55	4.02
S5	3.76	2.66	4.02
S6	3.76	2.78	4.02

The as-obtained products were characterized by X-ray diffraction (XRD, D/max-rA, Rigaku Corporation, Tokyo, Japan), field emission scanning electron microscope (FESEM, JEOL



Scheme 1 Schematic experimental setup for the synthesis of ZrN-Sialon composite powders and β -Sialon nanostructures.

JSM6700F, Japan), transmission electron microscopy (TEM/HRTEM, FEI-Tecnaï-G²-F20, Philips, Netherlands). The energy dispersive spectroscopies (EDS, HORIBA, 7593-H) linked with the SEM and the TEM were used to assist with the phase identification. Samples for TEM observation were dispersed in absolute ethanol by ultrasonication for 15 minutes, and a drop of the suspension containing the products was dropped onto a copper grid coated with an amorphous carbon supporting film and then dried in air. Fourier-transform infrared spectroscopy (FT-IR) data were collected on a Nicolet IR100/200 spectrophotometer over the wavenumbers range of 500-4000 cm^{-1} . The room temperature photoluminescence (PL) property of the products formed on the graphite felt were recorded with a fluorescence spectrophotometer (Hitach F-4600, Japan) from a Xe lamp excitation.

Results and discussion

In this research, β -Sialon nanostructures and ZrN-Sialon composite powders were synchronistic prepared by aluminothermic reduction nitridation method. Fig. 1a shows the XRD patterns and phase transformation of the composite powders

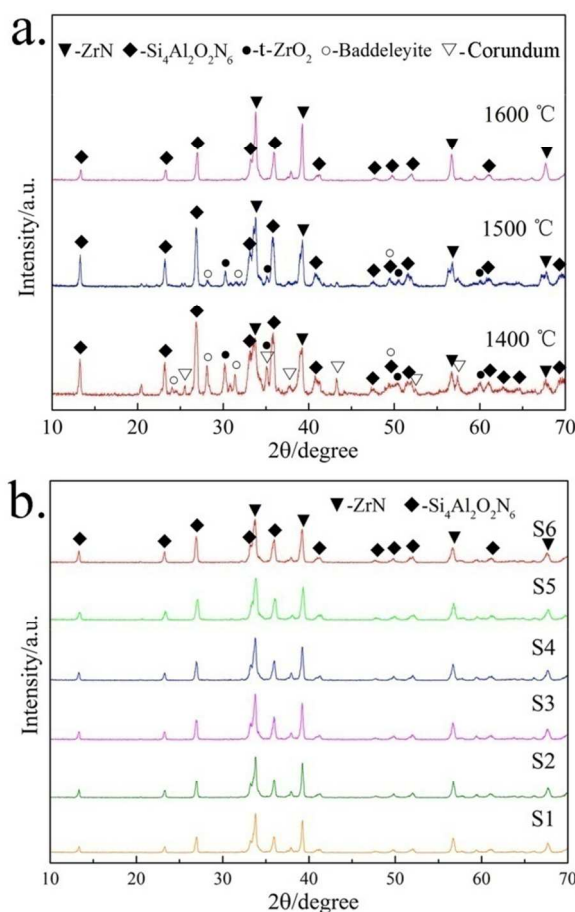


Fig. 1 The typical XRD patterns of the as-prepared samples via aluminothermic reduction nitridation in N_2 flow: (a) S1 at different temperatures for 4 h and (b) the composite powders synthesized by different aluminium contents at 1600 °C.

from S1 at 1400 °C, 1500 °C and 1600 °C for 4 h respectively. As Fig. 1a shows that ZrN and β -Sialon ($\text{Si}_4\text{Al}_2\text{O}_2\text{N}_6$, $z=2$) phases are formed at a relatively low temperature of 1400 °C accompanied with t-ZrO₂, baddeleyite and corundum. It can be inferred that zircon decomposed, ZrO₂ was partly nitride to ZrN and partly coexisted in the tetragonal phase and baddeleyite phase at this temperature. The corundum diffraction peaks are disappeared at the temperature of 1500 °C. With increasing the temperature to 1600 °C, ZrN and β -Sialon become the major phase. Fig. 1b shows the XRD patterns of samples with different aluminum contents after aluminothermic reduction nitridation at 1600 °C. All of the as-synthesized products mainly contain ZrN and β -Sialon ($\text{Si}_4\text{Al}_2\text{O}_2\text{N}_6$, $z=2$) phases.

Fig. 2 depicts the SEM images of the composite powders synthesized under different experimental conditions (a-b: S1 at 1400 °C; c-d: S1 at 1500 °C; e-f: S1 at 1600 °C) and the EDS spectrum record from the marked area A and B. The formation of the nanowires/nanobelts is quite evident from the images. Both nanowires and nanobelts are formed in the composite powders under different sintering temperatures. Furthermore, no catalyst tips are found at the tip of the nanostructures. It can also be seen from the images that the content of the nanostructures decreases with rising temperature. The content of the nanostructures in the composite powders can be tailored by temperature.

Fig. 2g and h are the EDS spectrum recorded from the nanostructures (the marked area A in Fig. 2b) and the particles (the marked area B in Fig. 2e). The EDS analysis reveals that the nanostructures formed in the composite powders are composed of Si, Al, O and N and the particles are composed of Zr, Si, Al, O and N. On account of the result, we roughly consider the nanostructures are β -Sialon. Fig. 2e is the SEM image taken from the sample S1 sintered at 1600 °C. As we can see from the XRD patterns (Fig. 1), the as-prepared composite powders sintered at 1600 °C mainly contain ZrN and β -Sialon. Combined with the EDS analysis, we consider the particles are composed of ZrN and β -Sialon. Except the composite powders, a white colored layer is formed on the surface of the graphite felt which is located around

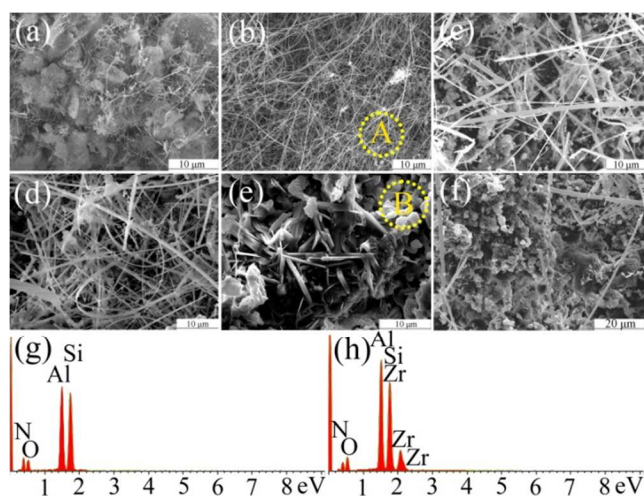


Fig. 2 The products synthesized under different experimental conditions. (a-b) S1 at 1400 °C; (c-d) S1 at 1500 °C; (e-f) S1 at 1600 °C; (g) EDS spectrum of the nanowires recorded from the marked area A in Fig. 2b; (h) EDS spectrum of the particles recorded from the marked area B in Fig. 2e.

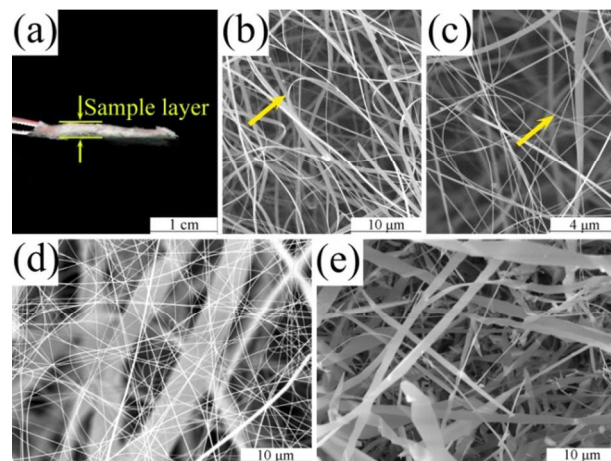


Fig. 3 (a) Digital camera photograph of the macroproducts synthesized on the graphite substrate; (b-e) Typical SEM images of the synchronistic formed nanobelts/nanowires at different temperatures: (b-c) 1400 °C; (d) 1500 °C; (e) 1600 °C.

the specimens (as shown in Scheme 1). Fig. 3a shows the digital camera photograph of the synchronistic formed products directly grown on the graphite felt around the samples without using catalysts. It reveals that a large scale white colored products have accumulated on the graphite substrate. The as-prepared white colored products were further characterized using SEM. Representative SEM images (Fig. 3b-c) revealed that the products synthesized at 1400 °C exhibit one-directional structures (nanobelts as shown in Fig. 3b and nanowires as shown in Fig. 3c). The length of the nanobelts/nanowires ranges from several to tens of microns. The width of the nanobelts is not of uniform size, which is ranged from 300 nm to 700 nm. The diameter of nanowires is 50-150 nm. To account for the effect of the temperature on the growth of the β -Sialon nanostructures, we also observed the products synchronistic formed at 1500 °C and 1600 °C. It is noticeable that all these mentioned three synchronicity formed products were taken around the similar sample S1 to make the as-grown nanostructures comparably. The typical image of the products prepared at 1500 °C is displayed in Fig. 3d. The nanobelts can be observed to be thicker and wider. This result suggested that the morphology of the nanobelts can be changed along with the temperature. Once the temperature is further increased up to 1600 °C, the nanostructures became disorderly and unsystematic (Fig. 3e). As we can see from Fig. 3b-e, the best nanobelt/nanowire growth in terms of morphology and yield was observed for the graphite felt substrate located in the temperature of 1400 °C.

Fig. 4a shows the XRD pattern of the white colored products synchronistic prepared at 1400 °C (the vertical axis used the Log scale). As Fig. 4a indicated, in addition to the peak from the graphite felt, the other peaks match well with the standard diffraction pattern of β -Sialon phase. The diffraction peaks indicate that the white colored products were crystalline. In addition, FT-IR is also used to confirm the composition of the nanostructures. Fig. 4b shows the FT-IR spectrum of the synchronistic formed nanostructures which is similar to the previously reported β -Sialon spectrum.⁴ The absorption peak at around 852-893 cm^{-1} corresponds to the Si-N stretching mode of

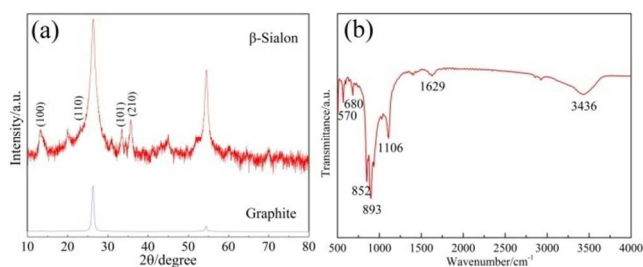


Fig. 4 (a) XRD pattern of the synchronistic formed nanobelts/nanowires; (b) FT-IR absorbance spectrum of the β -Sialon nanostructures.

corner-shared Si-N or Al-N tetrahedral structures.⁴ The peaks at around 570 cm^{-1} , 680 cm^{-1} and 1106 cm^{-1} can be assigned to the stretching frequency of the Si-O group, which points to Al-O partially replacing the Si-N bond in Sialon structures.⁴ There are two absorption peaks at around 1629 cm^{-1} and 3436 cm^{-1} , which corresponds to the N-O stretching vibration and Al-O stretching, respectively. Together with the XRD analyses, we believe that the synchronistic prepared nanostructures mainly consist of β -Sialon phase.

Further details of the internal structure and morphology of the as-synthesized nanostructures can be revealed by TEM and HRTEM, along with EDS. Fig. 5a depicts the TEM observation taken on several β -Sialon nanostructures and the EDS spectrum inset in Fig. 5a is record from a nanobelt. It can be confirmed in Fig. 5a that the as-prepared nanostructures are composed of nanobelts and nanowires and each nanobelt has a uniform width along its length. EDS pattern demonstrates that the products mainly contained Si, Al, O and N. The Cu and C peaks were from the copper grid used to support the sample. Fig. 5c displays a HRTEM image of the nanobelt shown in Fig. 5b, which shows that the nanobelt is structurally uniform without obvious defects. The measured d -spacing between two adjacent lattice fringes is 0.27 nm, match well with (101) plane of β -Sialon. The corresponding selected area electron diffraction (SAED) pattern of the nanobelt is shown in Fig. 5d. The diffraction spots clearly indicate the crystallized structure can also be indexed to crystalline β -Sialon. Both the lattice fringes and the SAED pattern indicate that the β -Sialon nanobelts are grown along the [001] direction. According to the TEM observations, EDS analysis and XRD pattern (Fig. 4), it is believed that the nanostructures were crystalline β -Sialon.

In the process of synthesizing 1-D nanostructures (nanowires, nanobelts, nanochains, nanorods, nanoneedles, etc.), vapor phase synthesis is probably the most extensively approach.² The vapor-solid (VS), vapor-liquid-solid (VLS), oxide-assisted growth mechanisms have been suggested for the vapor based methods. Generally, VS growth is believed to start at nanometric nuclei created *in situ* and the nuclei proceeds along one crystallographic direction.^{2, 28, 29} The growth of 1-D nanostructures without metal catalyst has been often demonstrated based on the VS process.³ Since no metallic catalyst was introduced and no metallic droplets were observed at the tips of the nanostructures, thus, it is plausible that the β -Sialon nanostructures growth is through VS mechanism.

In this work, the as-prepared nanostructures not only formed on the graphite substrate, but also existed in the composite

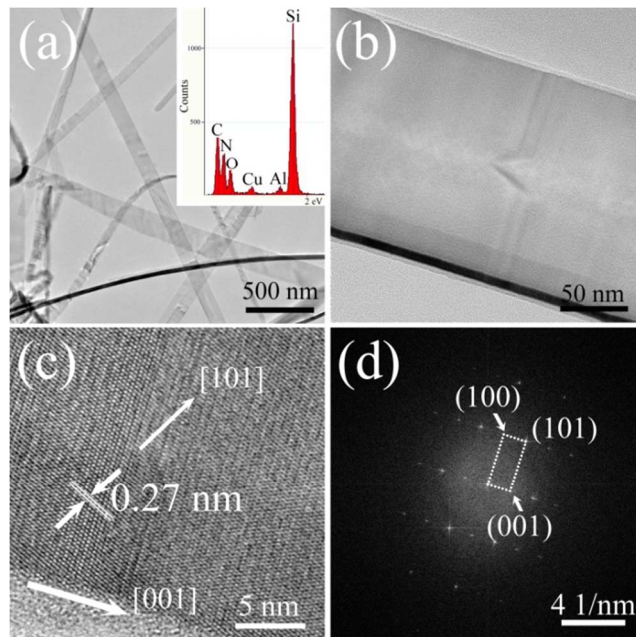
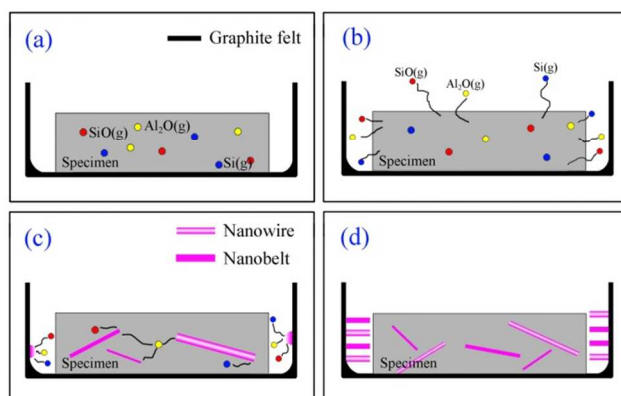


Fig. 5 (a) Low-magnification TEM image of the synchronistic prepared nanobelts/nanowires at 1400 °C (the inset is the EDS spectrum recorded from a nanobelt); (b) A typical TEM image of a single β -Sialon nanobelt; (c) HRTEM image of the crystalline nanobelt; (d) Corresponding SAED pattern of the nanobelt.

powders. Scheme 2 shows the proposed schematic illustration underpinning such a VS process. At first, ZrO_2 and SiO_2 are produced by the decomposition of zircon. At the experiment temperatures (1400 °C-1600 °C), vapor phases are formed in the specimens according to the reactions (2) to (6), as shown in Scheme 2a.



Scheme 2 Schematic illustration of the growth of β -Sialon nanostructures.

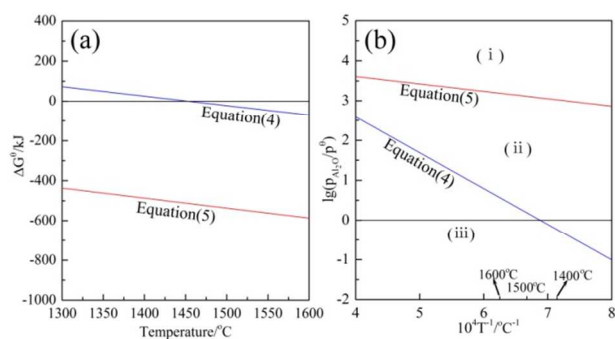
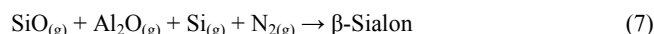


Fig. 6. (a) The Gibbs free energy (ΔG^θ) for reactions (4) and (5) between 1300 °C to 1600 °C; (b) Stable region of the condensed phases in the $\text{ZrO}_2\text{-SiO}_2\text{-Al-N}_2$ system when there is excess aluminum: (i) $\text{ZrO}_2(\text{s})+\text{SiO}_2(\text{s})+\text{Al}(\text{l})$; (ii) $\text{ZrO}_2(\text{s})+\text{Si}_4\text{Al}_2\text{O}_2\text{N}_6(\text{s})+\text{Al}(\text{l})$; (iii) $\text{ZrN}(\text{s})+\text{Si}_4\text{Al}_2\text{O}_2\text{N}_6(\text{s})+\text{Al}(\text{l})$.

With time going on, part of these vapor phases release from the specimens (Scheme 2b). When the pressure of SiO , Al_2O and Si vapors increase to a supersaturation condition, the generated vapors react further in the flowing N_2 system, according to reaction (7).



Based on the aforementioned reactions, β -Sialon nuclei are generated on the graphite felt and in the composite powders, as illustrated in Scheme 2c. The nuclei would grow along the length direction with the gaseous phases continued to diffuse to the tips (Scheme 2d). Although here we propose a growing mechanism, the above growth procedure of the nanobelts and nanowires is actually more complicated.

To investigate the phase transformation procedure in detail, the Gibbs free energies of the reaction system are calculated based on reactions (4) and (5). Table 2 shows the standard Gibbs free energies of reaction (4) and (5) (Fig. 6a shows the relationship between ΔG^θ and Temperature). To simplify to system, the partial pressure of N_2 (p_{N_2}) was assumed to equal to p^θ although the gaseous Al_2O and SiO existed. Thus, the values of $\lg(p_{\text{Al}_2\text{O}}/p^\theta)$ at different temperatures can be obtained from equation (8), where ΔG^θ represents standard Gibbs free energy, T represents temperature, K^θ means standard equilibrium constant and R means gas constant ($R=8.314\text{J}/(\text{mol}\cdot\text{K})$). The equilibrium relationship curves obtained by plotting $\lg(p_{\text{Al}_2\text{O}}/p^\theta)$ against $10^4/T$ are shown in Fig. 6b.

$$\Delta G^\theta = -RT \ln K^\theta \quad (8)$$

Table 2
Standard Gibbs free energies of reactions (4) and (5).

Reaction equation	Standard Gibbs free energy/ $\text{J} \cdot \text{mol}^{-1}$	$\lg(p_{\text{Al}_2\text{O}}/p^\theta)$
(4)	$\Delta_r G_4^\theta = 687640 - 473.28T$	$6.18 - 8980/T$
(5)	$\Delta_r G_5^\theta = 212830 - 499.58T$	$4.35 - 1853/T$

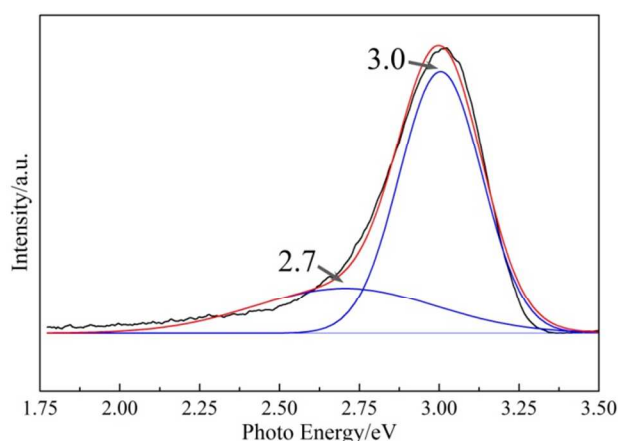


Fig. 7. The emission spectrum of the synchronistic synthesized β -Sialon nanobelts/nanowires (the black line is the as-obtained PL line, the red and the blue line is the simulated line).

According to Fig. 6a, it can be seen that equation (4) react at around 1400~1500 °C. ZrO_2 is initially and partially transformed to ZrN around this temperature (as illustrated in Fig. 1a). Equation (5) reacts at the whole experiment temperature region (1400~1600 °C) and no SiO_2 related phases remain in the product which is in agreement with the obtained results (as shown in Fig. 1). Fig. 6b is the equilibrium relationships of the condensed phases in the $\text{ZrO}_2\text{-SiO}_2\text{-Al-N}_2$ system. The stable regions of the condensed phases in the $\text{ZrO}_2\text{-SiO}_2\text{-Al-N}_2$ system are: (i) $\text{ZrO}_2(\text{s})+\text{SiO}_2(\text{s})+\text{Al}(\text{l})$; (ii) $\text{ZrO}_2(\text{s})+\text{Si}_4\text{Al}_2\text{O}_2\text{N}_6(\text{s})+\text{Al}(\text{l})$; (iii) $\text{ZrN}(\text{s})+\text{Si}_4\text{Al}_2\text{O}_2\text{N}_6(\text{s})+\text{Al}(\text{l})$. The thermodynamic data show that $\text{Si}_4\text{Al}_2\text{O}_2\text{N}_6$ can be generated directly by SiO_2 and Al , explains that platelike β -Sialon phase (Fig. 2e) can also be found in the composite powders.

To investigate the potential applications of the nanobelts/nanowires grown on the graphite substrate, photoluminescence (PL) measurement was performed at room temperature (Fig. 7). As shown in Fig. 7, the emission spectrum excited at 4.96 eV exhibited one emission peak centered at 3.02 eV. The black line is the as-obtained emission spectrum of β -Sialon nanobelts/nanowires, the red and blue line is the simulated lines. By using Acq Method, the black emission spectrum shows two emission peaks at 3.0 eV and 2.7 eV located in the violet/blue spectral range. Similar emission peaks at about 3.0 eV were also reported by Huang *et al.*⁶ for the β -Sialon nanobelts, which may be ascribed to the cation cavity and sublattices migration resultant from the replacement of the Si-N bond by the Al-O bond.⁴ The other weak emission peak at 2.7 eV might be caused by the emission of crystal stacking faults or other types of defects in the nanostructures. The PL property indicates that the β -Sialon nanobelts/nanowires prepared via aluminothermic reduction nitridation method may have potential applications in blue-light emitting diodes and display devices. Moreover, on account of the easy doping property of β -Sialon matrix, they will display different luminescence properties and demonstrate more extensive applications in optoelectronics.⁷⁻¹⁰

Conclusions

In conclusion, large scale β -Sialon nanobelts/nanowires were

prepared on the graphite substrate. The formation of the β -Sialon nanostructures was dominated by a vapor-solid (VS) mechanism and the photoluminescence spectrum of the nanostructures exhibits a significant violet-blue spectrum. Furthermore, ZrN-Sialon composite powders were synchronistic prepared via aluminothermic reduction nitridation at different conditions with flowing N_2 . The composite powders mainly contained granular ZrN and Sialon nanowires. The phase compositions and ratio of nanostructures to powder can be tailored by the experimental conditions. It is believed that the as-formed β -Sialon nanostructures can be valuable for future potential applications in blue-light emitting diodes and display devices and the novel powders can be useful for fabricating nanobelt/nanowire reinforced ceramic nanocomposites.

Acknowledgements

This work was supported by the National Natural Science Foundation of China (Grant No. 51032007, 51272241, 51472222 and 51372232) and the Research Fund for the Doctoral Program of Higher Education of China (Grant No. 20130022110006). Li Yin also thanks the Fundamental Research Funds for the Central Universities (Grant No. 2652014041). Haitao Liu thanks Fanrong Meng and Qing Li for their important contribution to this experiment as the first author.

Notes and references

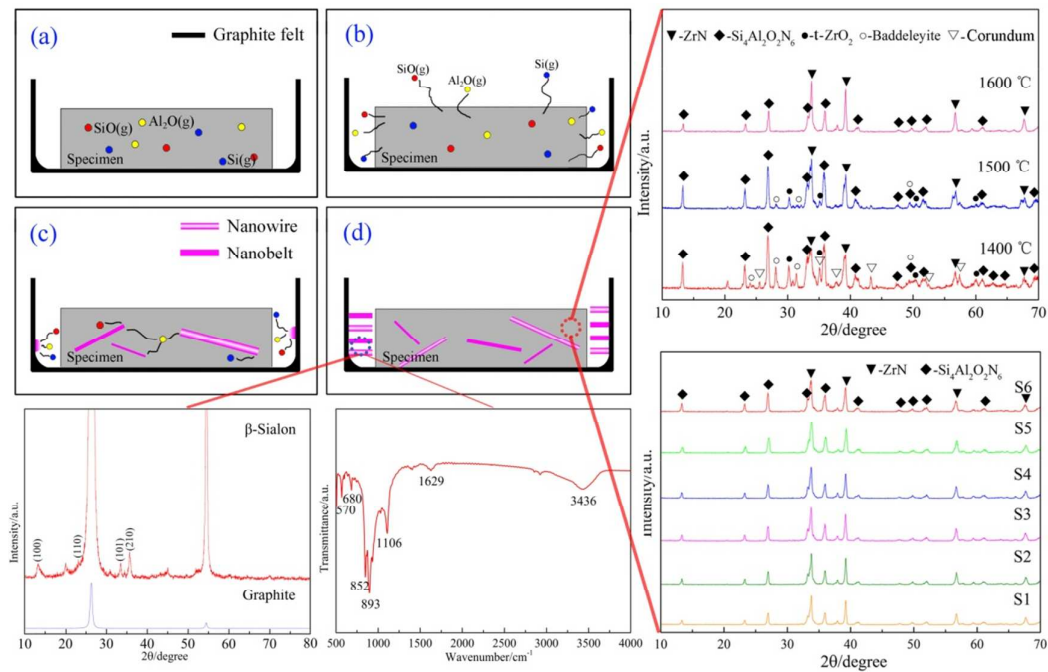
^a School of Materials Science and Technology, Beijing Key Laboratory of Materials Utilization of Nonmetallic Minerals and Solid Wastes, National Laboratory of Mineral Materials, China University of Geosciences(Beijing), 100083, P.R.China. Fax: +86 10 82322186; Tel: +86 10 82322186; E-mail: huang118@cugb.edu.cn.

^b School of Earth Sciences and Resources, China University of Geosciences, Beijing 100083, P.R.China.

^c Department of stomatology, Aviation Gmral Hospital, Beijing,100012, P. R. China.

^d Beijing Institutes of Life Science, Chinese Academy of Sciences, Beijing, 100101, P. R. China.

1. S. Iijima, *Nature*, 1991, **354**, 56.
2. Y. N. Xia, P. D. Yang, Y. G. Sun, Y. Y. Wu, B. Mayers, B. Gates, Y. D. Yin, F. Kim and H. Q. Yan, *Adv. Mater.*, 2003, **15**, 353.
3. H. T. Liu, Z. H. Huang, J. T. Huang, M. H. Fang, Y-G. Liu, X. W. Wu, *J. Mater. Chem. C.*, 2014, 2014, **2**, 7761.
4. C. L. Qin, G. W. Wen, X. Y. Wang, L. Song and X. X. Huang, *J. Mater. Chem.*, 2011, **21**, 5985.
5. K. Chen, M. H. Fang, Z. H. Huang, J. T. Huang and Y. G. Liu, *CrystEngComm*, 2013, **15**, 9032.
6. J. T. Huang, Y-G. Liu, Z. H. Huang, M. H. Fang, S. W. Zhang, W. Xie, J. Z. Yang, S. F. Huang and Y. G. Xu, *Cryst. Growth Des.*, 2012, **13**, 10.
7. J. T. Huang, H. P. Zhou, Z. H. Huang, G. H. Liu, M. H. Fang and Y-G. Liu, *J. Am. Ceram. Soc.*, 2012, **95**, 1871.
8. T. Suehiro, N. Hirosaki, R-J. Xie, M. Mitomo, *Chem. Mater.*, 2005, **17**, 308.
9. R-J. Xie, N. Hirosaki, M. Mitomo, Y. Yamamoto, T. Suehiro and K. Sakuma, *J. Phys. Chem. B*, 2004, **108**, 12027.
10. L-O. Nordberg, Z. J. Shen, M. Nygren and T. Ekström, *J. Eur. Ceram. Soc.*, 1997, **17**, 575.
11. J. T. Huang, Z. H. Huang, Y. G. Liu, M. H. Fang, K. Chen, Y. T. Huang, S. F. Huang, H. P. Ji, J. Z. Yang, X. W. Wu and S. W. Zhang, *Nanoscale*, 2014, **6**, 424.
12. P. L. Dong, X. D. Wang, M. Zhang, M. Guo and W. C. Li, *Sci. China Ser. E*, 2009, **52**, 3122.
13. Z. J. Shen, Z. Zhao, H. Peng and M. Nygren, *Nature*, 2002, **417**, 266.
14. A. Ziegler, J. C. Idrobo, M. K. Cinibulk, C. Kisielowski, N. D. Browning and R. O. Ritchie, *Science*, 2004, **306**, 1768.
15. M. G. Nicholas, D. A. Mortimer, L. M. Jones and R. M. Crispin, *Science*, 1990, **25**, 2679.
16. Y. Kurokawa, K. Utsumi and H. Takamizawa, *J. Am. Ceram. Soc.*, 1988, **71**, 588.
17. J. T. Huang, S. W. Zhang, Z. H. Huang, Y-G. Liu and M. H. Fang, *CrystEngComm*, 2013, **15**, 785.
18. J. Kim, A. Rosenflanz and I. W. Chen, *J. Am. Ceram. Soc.*, 2000, **83**, 1819.
19. Y. T. Li, Z. H. Huang, Y. G. Xu, M. H. Fang, Y-G. Liu, J. Z. Yang and X. Z. Hu, *Mater. Res. Bull.*, 2012, **47**, 3273.
20. L. Yin, Y. G. Xu, Z. H. Huang, Y-G. Liu, M. H. Fang and B. L. Liu, *Powder Technol.*, 2013, **246**, 677.
21. K. Schwarz, A. R. Williams, J. J. Cuomo, J. H. E. Harper and H. T. G. Hentzell, *Phys. Rev. B*, 1985, **32**, 8312.
22. X. J. Zhao, D. L. Chen, H. Q. Ru and N. Zhang, *J. Eur. Ceram. Soc.*, 2011, **31**, 883.
23. F. Monteverde and A. Bellosi, *Scripta Mater.*, 2002, **46**, 223.
24. L. Kvetková, A. Duszová, P. Hvizdoš, J. Dusza, P. Kun and C. Balázs, *Scripta Mater.*, 2012, **66**, 793.
25. K. G. Dassios, D. G. Aggelis, E. Z. Kordatos and T. E. Matikas, *Compos. Part A: Appl. S.*, 2013, **44**, 105.
26. J. Magnant, R. Pailler, Y. Le Petitcorps, L. Maillé, A. Guette, J. Marthe and E. Philippe, *J. Eur. Ceram. Soc.*, 2013, **33**, 181.
27. C. D. Li, Z. F. Chen, J. X. Zhu, Y. Liu, Y. Jiang, T. R. Guan, B. B. Li and L. Lin, *Mater. Design*, 2012, **36**, 289.
28. Y. D. Yin, F. Kim and H. Q. Yan, *Adv. Mater.*, 2003, **15**, 353.
29. K. Zekentes, K. Rogdakis, *J. Phys. D: Appl. Phys.*, 2011, **44**, 133001.
30. M. Ksiazek, N. Sobczak, B. Mikulowski, W. Radziwill and I. Surowiak, *Mat. Sci. Eng: A*, 2002, **324**, 162.
31. X. S. Fang, C. H. Ye, L. D. Zhang and T. Xie, *Adv. Mater.*, 2005, **17**, 1661.



Highlight:

Large scale β -Sialon nanobelts/nanowires and ZrN-Sialon composite powders were prepared via aluminothermic reduction nitridation with flowing N_2 .